

Boosting the Performance of a Lipkin-Meshkov-Glick Quantum Battery via Symmetry-Breaking Quenches and Bosonic Baths

Le Bin Ho,^{1, 2, 3,*} Duc Tuan Hoang,⁴ Tran Duong Anh-Tai,^{4, 5, 6} Thomas Busch,⁴ and Thomás Fogarty⁴

¹*Frontier Research Institute for Interdisciplinary Sciences, Tohoku University, Sendai 980-8578, Japan*

²*Department of Applied Physics, Graduate School of Engineering, Tohoku University, Sendai 980-8579, Japan*

³*Theoretical Sciences Visiting Program, Okinawa Institute of Science and Technology Graduate University, Onna, 904-0495, Japan*

⁴*Quantum Systems Unit, OIST Graduate University, Onna, Okinawa 904-0495, Japan*

⁵*Homer L. Dodge Department of Physics and Astronomy,*

The University of Oklahoma, 440 W. Brooks Street, Norman, Oklahoma 73019, USA

⁶*Center for Quantum Research and Technology, The University of Oklahoma,*

440 W. Brooks Street, Norman, Oklahoma 73019, USA

(Dated: February 20, 2026)

We explore the operation of quantum batteries in the Lipkin-Meshkov-Glick (LMG) model, when they are charged either through a sudden quench in the magnetic field strength or by coupling them to a bosonic oscillator bath. Through initializing the battery in either the symmetric or broken symmetry phases of the LMG model we analyze how the different spectral properties can affect the performance of both the charging and discharging of the battery. In particular, we show that by quenching the magnetic field strength from the symmetric phase to the broken phase, we can achieve a significant enhancement in stored energy, as well as stable and efficient ergotropy extraction. Similar observations can be made when introducing weak coupling between the battery with the bosonic bath, while the amount of stored work and ergotropy saturate at strong coupling. These findings emphasize the importance of the magnetic field dynamics and environmental coupling in optimizing charging performance, which could lead to practical applications in quantum energy storage.

I. INTRODUCTION

In the epoch of the second quantum revolution, quantum batteries (QBs) are emerging as a promising energy-storage innovation for advancing quantum technologies, particularly for applications necessitating quick charging of quantum devices with high energy-conversion efficiency. In contrast to classical batteries which rely predominantly on chemical compounds, QBs harness quantum properties such as entanglement and coherence to surpass their classical counterpart in various aspects, such as charging and discharging performances, and energy capacity [1, 2].

Over the last couple of years, various QB models have been proposed, each possessing distinct strengths and limitations. Early studies have focused on many-body systems, such as the Dicke model [3–8], the Sachdev-Ye-Kitaev model [9, 10], and spin-chains [11–30]. These models aim to enhance charging efficiency through collective quantum effects [3, 4, 17], entanglement [4, 7, 31–33], non-Hermitian terms [34], noise-assisted fast charging [35, 36], and optimal control [37–40]. Recent QB designs, such as those based on cavity quantum electrodynamics (cavity QED), utilize strong coupling between qubits and cavity modes [41], incorporate memory effects [42], and repeated interactions [43] to improve energy storage and charging efficiency. However, achieving a balance

between efficiency, robustness, and scalability poses significant challenges. For instance, quantum decoherence restricts expanding the size of these batteries, while limited degrees of freedom in the charger prevent full saturation, which decreases the energy transfer efficiency. Theoretical studies on QBs have thus far examined numerous mechanisms to enhance performance. These include nonreciprocal energy transfer to reduce losses [44], the derivation of upper limits for energy storage [44, 45], the use of (non)completely positive trace-preserving maps [46], and the exploration of causal order effects [47]. Some studies have integrated topological properties to increase the robustness against noise [30, 48]. Furthermore, experimental investigations of QBs have been conducted using nuclear magnetic resonance (NMR) systems with star topology and photonic platforms [47, 49, 50]. Although these approaches demonstrate distinct advantages compared to classical systems, practical challenges, such as complex initialization and control, remain significant limitations.

In this work, we introduce and analyze a QB based on the Lipkin-Meshkov-Glick (LMG) model, which is a many-body spin system originally studied in nuclear physics [51–53]. From the theoretical perspective, the LMG model has gained attention in the field of quantum thermodynamics due to its collective long-range spin interactions [54] and second-order phase transition [55–61]. Furthermore, it can be solved exactly using the algebraic Bethe ansatz [62, 63] or by mapping angular momentum operators to N Schwinger bosons in the weak interaction limit [64]. In the thermodynamic limit, the

* Electronic address: binho@fris.tohoku.ac.jp

Holstein-Primakoff transformation provides an exact solution [60, 65, 66]. It is interesting to remark that near the critical point this system exhibits enhanced sensitivity, a characteristic that has been widely explored in quantum sensing, metrology and speed limits [67–72]. Some preliminary works on the LMG model have shown that quantum entanglement can boost charging power [45], while shortcuts to adiabaticity further improve charging speed and overall performance [73]. More importantly, the LMG model has already been experimentally implemented in trapped ions [74–77] and ultracold quantum gases [78–80]. Overall, these features therefore make the LMG model a compelling candidate for energy storage and energy extraction, with the potential for improved charging efficiency and robustness against decoherence.

In this study, we systematically investigate the charging protocols of QB by suddenly quenching it across the critical point, or by connecting it to a bosonic bath. By quenching the magnetic field from the symmetric phase to the broken symmetry phase and introducing coupling with a bosonic bath, we observed a significant improvement in stored energy, along with stable and efficient ergotropy extraction. Our results highlight the magnetic field dynamics and environmental coupling as key factors in optimizing charging performance for QBs.

The manuscript is structured as follows. Section II outlines the theoretical framework and setup for the LMG-based QB. We presents the main findings of our study in Section III. Finally, the conclusions encompassing a discussion of the implications and potential applications of this approach in quantum energy storage technologies are drawn in Section IV. To simplify notations, we shall refer to the battery Hamiltonian as H_B and the charging Hamiltonian as H_C throughout this work.

II. THEORETICAL FRAMEWORK

A. The LMG model

To model the QB, we consider an ensemble of N spin- $\frac{1}{2}$ particles with all-to-all interactions characterized by the LMG Hamiltonian [51–53]

$$H_{\text{LMG}} = \frac{\lambda}{N} \sum_{i < j}^N \left(\sigma_x^i \sigma_x^j + \gamma \sigma_y^i \sigma_y^j \right) + h \sum_{i=1}^N \sigma_z^i, \quad (1)$$

where σ_α are the Pauli matrices with $\alpha = x, y, z$. Here, λ and h denote the spin-spin coupling strength, and the strength of the external magnetic field, respectively. The anisotropy parameter γ can range from 0 (fully anisotropic) to 1 (fully isotropic). It has been proven that the LMG model exhibits a second-order quantum phase transition (QPT) driven by the interplay between the spin-spin interactions and the external magnetic field [55–61]. In the thermodynamic limit ($N \rightarrow \infty$), when

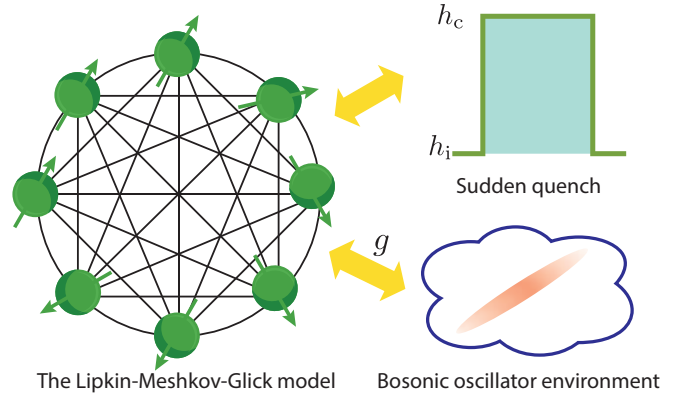


FIG. 1. An LMG-based QB featuring full-range interactions between spin-1/2 particles. The charging process is employed through (1) sudden quenching of the external magnetic field, (2) coupling to a bosonic oscillator environment.

$h > \lambda$, the spins align with the external magnetic field, resulting in spontaneous magnetization. Meanwhile, for $h < \lambda$, the interaction energy dominates, leading to a two-fold degenerate energy spectrum. The symmetry breaking occurs at the critical point $h = \lambda$, separating the symmetric phase ($h > \lambda$) from the symmetry-broken phase ($h < \lambda$). Throughout this study, we will focus on the ferromagnetic case ($\lambda > 0$) and set $\lambda = 1$ for simplicity.

For the analysis of the LMG-based QB, one needs the complete energy spectrum and the corresponding eigenstates of the Hamiltonian Eq. (1). For numerical purposes, it is convenient to rewrite the LMG Hamiltonian given by Eq. (1) in terms of the collective spin operators, $J_\alpha = \frac{1}{2} \sum_i \sigma_\alpha^{(i)}$, which can then be recast as

$$H_{\text{LMG}} = \frac{2}{N} \left(J_x^2 + \gamma J_y^2 \right) + 2h J_z. \quad (2)$$

Due to the permutation invariance of the collective spin system [54], i.e., the total angular momentum \mathbf{J} is conserved, $[\mathbf{J}, H_{\text{LMG}}] = 0$, we only focus on the maximum angular momentum $j_{\text{max}} = N/2$, resulting in a Hilbert space of dimension $d = N+1$. The matrix elements of the Hamiltonian Eq. (2) are known analytically in the Dicke basis $|N/2, m\rangle \equiv |m\rangle$ with $-N/2 \leq m \leq N/2$ and the matrix can then be numerically diagonalized. Further details on the derivation of Eq. (2) and the numerical methodology are presented in Appendix A.

B. Charging protocols

In this section, we outline two different charging strategies for an LMG-based QB which are schematically illustrated in Fig. 1.

1. Charging by sudden quench of the magnetic field

Initially, the QB is assumed to be in the ground state $|\varepsilon_0\rangle$ of the LMG Hamiltonian, $H_B = H_{\text{LMG}}(h_i)$, with magnetic field strength h_i and with initial energy ε_0 . To charge the QB, the magnetic field is abruptly changed from the initial value h_i to a value $h_c \neq h_i$ at time $t = 0$, leading to the creation of out-of-equilibrium dynamics that excites the system to higher energy levels, thereby injecting energy into the QB. As the post-quench dynamics of the QB is governed by the charging Hamiltonian $H_C = H_{\text{LMG}}(h_c)$, the charging performance can be optimized by adjusting the magnetic field strength h_c along with the initial magnetic field strength h_i . Our aim is to examine the role of the different phases of the LMG model on both charging and discharging the battery. Specifically, whether quenching within the same phase, or between the phases, can result in more powerful and stable battery performance.

2. Charging by coupling to a bosonic oscillator bath

In the second strategy, the QB is charged by connecting it to a bosonic reservoir. Specifically, we consider the QB being prepared in the ground state of the LMG Hamiltonian, $H_B = H_{\text{LMG}}(h_i)$, while the charging Hamiltonian is given by

$$H_C = H_{\text{LMG}}(h_i) + H_{\text{bath}} + H_{\text{coupling}}. \quad (3)$$

The coupling between the LMG-based QB and a bosonic oscillator bath is modeled as

$$H_{\text{coupling}} = g(J_+a + J_-a^\dagger), \quad (4)$$

where g denotes the coupling strength between the QB and the bath. The bath Hamiltonian is described by $H_{\text{bath}} = \omega a^\dagger a$ with a^\dagger and a being the bosonic creation and annihilation operators corresponding to a photon with frequency ω . Here $J_\pm = J_x \pm iJ_y$ are the collective spin raising and lowering operators, respectively (see Appendix A for details). To fully charge the QB via the coupling in Eq. (4), the bath must supply sufficient energy to populate the battery's maximum excited manifold (i.e., its full capacity). This is achieved by preparing the bath in the Fock state $|n\rangle$ with $n \geq N$ [1, 4, 45]. Note that while many protocols assume this condition in practice, it is not a universal thermodynamic constraint that the bath energy needs to strictly exceed the QB energy for all coupling models [4], so throughout this work we set $n = N$.

C. Quantities of interest

At time t , the energy of the QB is defined as the expectation value of H_B with respect to the time-evolving

state $|\psi(t)\rangle = \exp(-iH_C t)|\psi_0\rangle$

$$E(t) = \langle\psi(t)|H_B|\psi(t)\rangle, \quad (5)$$

where $|\psi_0\rangle$ is the initial state, i.e., $|\psi_0\rangle = |\varepsilon_0\rangle$ for the quenching case and $|\psi_0\rangle = |\varepsilon_0\rangle \otimes |n\rangle$ for the coupling case.

The total work stored in the entire QB is given by

$$\mathcal{W}(t) = E(t) - \varepsilon_0. \quad (6)$$

The power can therefore be defined as

$$\mathcal{P}(t) = \frac{\mathcal{W}(t)}{t}. \quad (7)$$

It is worth noting that only a certain amount of the total work is necessarily accessible, especially when extracting work from only a subset of battery cells. When focusing on $0 < M \leq N$ cells, this partial discharge might be due to limitations in accessing the full state of the system or intentionally leaving part of the battery charged. In such cases, energy can remain “locked” in correlations between the M active cells and the $N - M$ inactive ones, reducing the total amount of extractable work. Consider an M -cell subsystem with the Hamiltonian

$H_B^M = \sum_{i=1}^M \zeta_i |\zeta_i\rangle\langle\zeta_i|$, with $\zeta_i < \zeta_{i+1}$ and its quantum state at time t is given by

$$\rho^M(t) = \text{Tr}_{N-M} [|\psi(t)\rangle\langle\psi(t)|] = \sum_{j=1}^M \eta_j(t) |\eta_j(t)\rangle\langle\eta_j(t)|, \quad (8)$$

with $\eta_j(t) \geq \eta_{j+1}(t)$ being the eigenvalues sorted in descending order. The ergotropy $\mathcal{E}(t)$ of the M -cell subsystem with respect to H_B^M quantifies the maximum extractable work extracted from $\rho^M(t)$ via a unitary transformation

$$\mathcal{E}(t) = \text{Tr}[\rho^M(t)H_B^M] - \text{Tr}[\sigma^M(t)H_B^M], \quad (9)$$

where $\sigma^M(t)$ is a passive state associated with $\rho^M(t)$, defined as

$$\sigma^M(t) = \sum_{i=1}^M \eta_i(t) |\zeta_i\rangle\langle\zeta_i|. \quad (10)$$

This definition ensures that the passive state $\sigma^M(t)$ possesses a minimum energy, known as the passive energy, thereby preventing any further work from being extracted from $\rho^M(t)$ via unitary operations [1]. The ergotropy $\mathcal{E}(t)$ therefore can be written in the form

$$\mathcal{E}(t) = \sum_{i=1}^M [p_i(t) - \eta_i(t)] \zeta_i, \quad (11)$$

where

$$p_i(t) = \sum_{j=1}^M \eta_j(t) |\langle\eta_j(t)|\zeta_i\rangle|^2, \quad (12)$$

is the population of $\rho^M(t)$ in the eigenbasis of H_B^M . It is apparent that the differences between the populations $p_i(t)$ and $\eta_i(t)$ are required for finite work extraction from M active cells. The M -cell stored work \mathcal{W}^M is therefore given as

$$\mathcal{W}^M(t) = \text{Tr}[\rho^M(t)H_B^M] - \text{Tr}[\rho^M(0)H_B^M], \quad (13)$$

where $\rho^M(0)$ is the initial state of the M -cell subsystem. Note that in general, the ergotropy \mathcal{E} and the M -cell stored work \mathcal{W}^M satisfy the relation $\mathcal{W}^M \geq \mathcal{E}$ with the fact that the equality only holds just when $\rho^M(t)$ represents a pure state.

It is important to remark that we will trace out $N - M$ cells to construct $\rho^M(t)$ when examining the charging strategy through magnetic field quenching in section III A. Meanwhile we only trace out the bath and investigate the entire N -cell battery in the second strategy via the coupling to a bosonic bath in section III B.

III. RESULTS AND DISCUSSION

A. Charging by quenching the external magnetic field

In this section, we will discuss the charging protocol for the LMG QB by quenching the magnetic field, which is experimentally feasible. We remark that in the following, our analysis focuses on the anisotropic case ($\gamma = 0$) since the system can be excited easily during the charging process and thus store energy more efficiently. In Appendix B, we demonstrate that the LMG model in the isotropic case ($\gamma = 1$) is not a good candidate for realizing QBs as the excitations are mostly suppressed in the broken phase ($h < \lambda$). For the analysis below, we consider $N = 100$ spin-1/2 particles with other parameters specified in each case.

1. The excitation energy spectrum

First, let us analyze the excitation energy spectrum of the LMG model in the anisotropic case, which will provide the understanding of how much energy can be stored in the battery and its dynamical properties. Let us denote $\{|\varepsilon_l\rangle\}$ and $\{\varepsilon_l\}$ the eigenstates and eigenvalues of H_B ; and $\{|\mu_k\rangle\}$ and $\{\mu_k\}$ are the eigenstates and eigenvalues of H_C .

In Fig. 2(a), we show the energy gap between the ground state and low-lying excited states, $\varepsilon_l - \varepsilon_0$. When $h_i \gtrsim 0.9$, the system is in the symmetric phase with non-degenerate energy levels. For $h_i < 0.9$, the system transitions to the broken phase, where certain gaps close, creating two-fold degeneracies, consistent with Ref. [58]. The critical value of h_i varies with the energy ε_l , and the set of these critical values defines the boundary between the symmetric and broken phases. Fig. 2(b) presents the

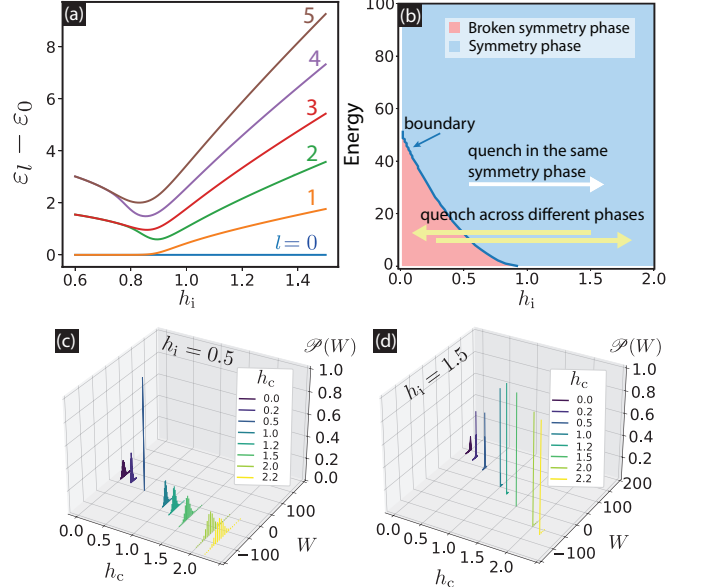


FIG. 2. (a) Energy gap between the ground state and the first five excited states as a function of the magnetic field h_i for $N = 100$ particles in the anisotropic case $\gamma = 0$. (b) Phase diagram showing the boundary between the symmetric and broken phase, including cases of quenches within the same phase and across different phases. (c,d) Work probability distribution $\mathcal{P}(W)$ with different h_c for (c) $h_i = 0.5$ and (d) $h_i = 1.5$.

phase diagram for $N = 100$ and in the following we will consider both quenches within the same phase and between different phases.

2. Work probability distribution function

To deepen our understanding of the charging process, we must analyze the distribution of excitations in the eigenbasis of the charging Hamiltonian H_C after the magnetic field quench. This can be conveniently quantified by the work probability distribution (WPD) [81, 82]

$$\mathcal{P}(W) = \sum_k |\langle \mu_k | \varepsilon_0 \rangle|^2 \delta(W - (\mu_k - \varepsilon_0)), \quad (14)$$

which quantifies the probability of doing some work W on the system and gives additional insight into how energy is injected into the QB during the charging process.

In Fig. 2(c) we show the WPD for an initial state being in the broken phase $h_i = 0.5$. In this case, the system can be excited into broad distributions of different energy eigenstates whether quenched within the same broken symmetry phase $h_c < 0.9$ or quenched across the critical point into the symmetric phase $h_c > 0.9$ [58]. The wide spread of the WPD when the initial state is prepared in the broken phase indicates that quenching in either direction creates ample excitations in the QB state that could be extracted at a later time.

In stark contrast, when the system is initiated in the symmetric phase, we can see that $\mathcal{P}(W)$ strongly depends on the quench direction as shown in Fig. 2(d) for the specific case $h_i = 1.5$. For quenches within the symmetric phase ($h_c > 0.9$), the WPD is extremely localized with a single predominant peak which corresponds to the system remaining in the ground state of the post-quench Hamiltonian, i.e. $|\langle \varepsilon_0 | \mu_0 \rangle|^2 \approx 1$, and there are scant excitations to higher energy eigenstates. Therefore, negligible charging transpires for quenches within the symmetric phase which is due to the fact that the spins are well-oriented by the magnetic field, leading to an absence of interactions and no buildup of many-body excitations. However, for quenches to the broken phase (for instance $h_c < 0.9$), the interaction between spins becomes dominant and the work distribution broadens, signifying an increased energy contribution once $h_c \rightarrow 0$ as depicted in Fig. 3 which we will discuss in the next section.

3. Stored energy, entropy, and power

We explore the total work stored $\mathcal{W}(t)$ in the battery state at the end of the charging process as calculated from Eq. (6). Explicitly, it is given by

$$\mathcal{W}(t) = \sum_l \left| \sum_k \exp(-i\mu_k t) \langle \mu_k | \varepsilon_0 \rangle \langle \varepsilon_l | \mu_k \rangle \right|^2 (\varepsilon_l - \varepsilon_0). \quad (15)$$

Furthermore, we will employ the long-time averaged work

$$\langle \mathcal{W} \rangle = \sum_l \sum_k |\langle \mu_k | \varepsilon_0 \rangle|^2 |\langle \varepsilon_l | \mu_k \rangle|^2 (\varepsilon_l - \varepsilon_0), \quad (16)$$

and its variance

$$\text{Var}(\mathcal{W}) = \sum_{l,l'} \sum_k |\langle \mu_k | \varepsilon_0 \rangle|^2 |\langle \varepsilon_l | \mu_k \rangle|^2 |\langle \varepsilon_{l'} | \mu_k \rangle|^2 \times (\varepsilon_l - \varepsilon_0)(\varepsilon_{l'} - \varepsilon_0) - \left[\sum_l \sum_k |\langle \mu_k | \varepsilon_0 \rangle|^2 |\langle \varepsilon_l | \mu_k \rangle|^2 (\varepsilon_l - \varepsilon_0) \right]^2, \quad (17)$$

to evaluate the effectiveness of the charging protocols (see Appendix C for the derivation).

Broken phase: We first discuss initializing the QB in the broken phase with $h_i = 0.5$ and then quench to different final values of the magnetic field strength h_c . The stored work in the QB is shown in Fig. 3(a) as a function of the charging time for representative values of h_c . Quenching within the same phase ($h_c < h_i$) the average work $\mathcal{W}(t)$ has large oscillations which slowly decay [blue and orange curves in Fig. 3 (a)]. When no quench occurs ($h_c = h_i = 0.5$), there is no energy gain and therefore $\mathcal{W}(t) = 0$. In contrast, quenching across the critical point ($h_c = 1.5, 2.0, 2.2$) results in faster oscillations and a quicker saturation of the stored work.

This behavior is also reflected in the dynamics of the Shannon entropy shown in Fig. 3(b), which allows us to quantify how spread the energy population is in the battery Hamiltonian. It is defined as

$$S(t) = - \sum_i p_i(t) \ln p_i(t), \quad (18)$$

where the populations p_i are given in Eq. (12) for $M = N$. When no quench occurs ($h_c = h_i = 0.5$), the entropy remains zero, consistent with the absence of energy gain. In contrast, when the system is quenched, the entropy increases and exhibits oscillations. This indicates that the system explores a broader set of excited states, which is consistent with the enhanced work storage observed in Fig. 3(a) and the work probability distribution shown in Fig. 2 (c). Thus, the entropy dynamics reinforce the work analysis: quenching drives the system deeper into the excited spectrum, enabling more efficient charging regardless of the direction of the quench, $h_c < h_i$ or $h_c > h_i$.

To clarify the effectiveness of the charging of the LMG battery over the entire operation range of h_c , we show the maximum work \mathcal{W}_{\max} and the average work $\langle \mathcal{W} \rangle$ in Fig 3(c). Quenching to smaller magnetic field strengths $h_c < h_i$ results in larger values of maximum work and its time average when compared to quenching to larger magnetic field strengths $h_c > h_i$. After the critical point at $h_c \approx 0.9$ the time-averaged work only slowly increases with increasing magnetic field strength, appearing to saturate when driven deep into the symmetric phase. We also note that the standard deviation of the stored work, indicated by the light blue shaded region, possesses larger values in this regime, indicating increased fluctuations of the energy that is stored in the battery.

Finally, we analyze the maximum power \mathcal{P}_{\max} and the optimal charging time t_{opt} , as shown in Fig. 3(d). The results show that \mathcal{P}_{\max} is small when the quench is performed within the same broken phase but increases significantly when the system is quenched into the symmetric phase. At the same time, t_{opt} decreases monotonically as h_c increases. This is due to quenches within the broken phase creating slow oscillations, resulting in a large t_{opt} and a small \mathcal{P}_{\max} . In contrast, quenching into the symmetric phase induces faster oscillations, producing a smaller t_{opt} and a much larger \mathcal{P}_{\max} .

Symmetric phase: Next, we discuss preparing the battery in the symmetric phase with $h_i = 1.5$ and again quenching to the new magnetic field strength h_c . The stored work $\mathcal{W}(t)$ is shown in Fig. 3(e), and immediately it is clear that the behavior of the battery is drastically different. When quenching within the symmetric phase, $\mathcal{W}(t)$ oscillates without decaying, with vanishingly small values as shown in the inset. This is consistent with the analysis of the work probability distribution in Fig. 2(d) and the entropy as shown in Fig. 3(f), as quenches within the symmetric phase do not create many excitations and therefore the amount of charge in the QB state is minimal.

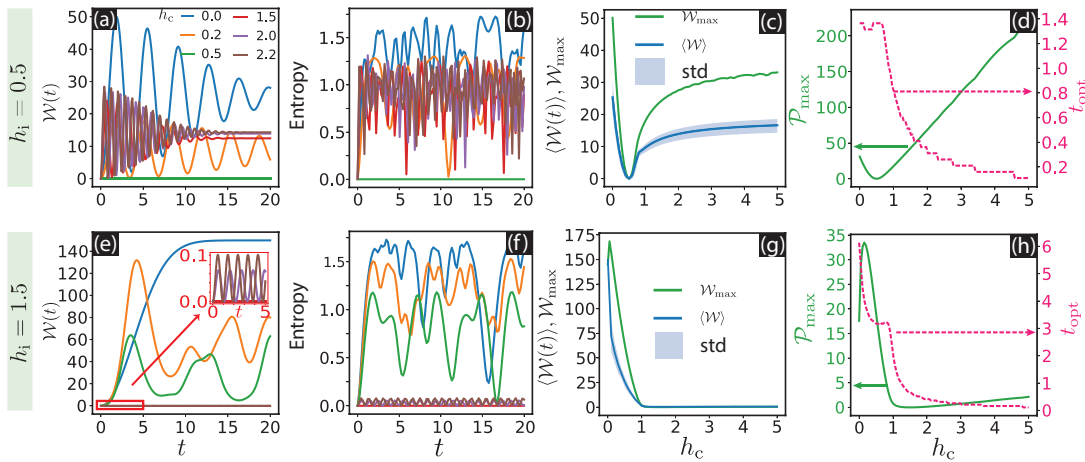


FIG. 3. Time evolution of the total stored work $\mathcal{W}(t)$ (a,e) and entropy (b,f). (c,d) Dependence of the maximum stored work, \mathcal{W}_{\max} , the long-time averaged work $\langle \mathcal{W} \rangle$ and its standard deviation ($\sqrt{\text{Var}(\mathcal{W})}$) on the quench parameter h_c . (d,h) Variation of the peak power, \mathcal{P}_{\max} , and the optimal charging time, t_{opt} , as functions of h_c , illustrating contrasting dynamical behaviors. The first and second rows represent the initial state being in the broken phase ($h_i = 0.5$) and the symmetric phase ($h_i = 1.5$), respectively. The inset in panel (e) magnifies the interval $0 \leq t \leq 5$, highlighting short-time dynamics.

However, significant features appear when quenching across the phase boundary from the symmetric to the broken phase. The further the system is driven into the broken phase the more work is stored in the QB. For finite magnetic field strengths $h_c \neq 0$, the maximum of the work is quickly reached before displaying complex oscillations. However, in the limit $h_c = 0$, $\mathcal{W}(t)$ increases at a slower rate but eventually saturates to a large and constant value. We note that in this case the maximum and average work are equivalent as seen in Fig. 3(g), as the variance of the stored work effectively vanishes, displaying a significant charging advantage. Again, this analysis is consistent with the work probability distribution shown in Fig. 2(d) and the entropy as shown in Fig. 3(f), as the energy is distributed over a larger region of the Hilbert space when quenched deeper into the broken phase, leading to significantly larger energy storage when compared to $h_i = 0.5$. Lastly, we note that while more work can be stored in this QB, it requires longer charging times which reduces the power, as shown in Fig. 3(h).

4. Extracted energy

To explore the role of correlations on the amount of energy that can be extracted from the QB, we calculate the ergotropy \mathcal{E} given by Eq. (11) for a subsystem of $M \leq N$ spins. Quantum correlations between these M spins and the remaining $N - M$ spins of the total system will lead to a reduction of the ergotropy with respect to the amount of work \mathcal{W}^M stored in this subsystem given by Eq. (13). We can therefore define the ratio between the ergotropy and the work, $\mathcal{E}/\mathcal{W}^M$, as a quantifier of the efficiency of the energy extraction process, saturating to unity when no correlations are present.

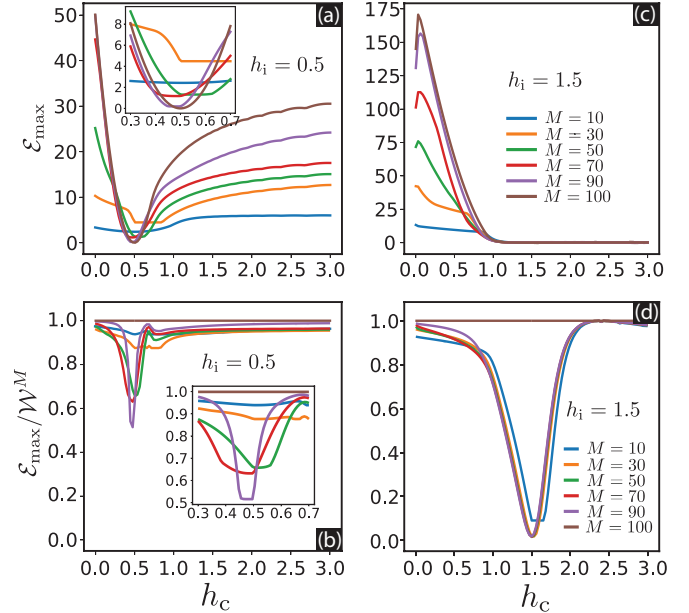


FIG. 4. The maximum ergotropy \mathcal{E}_{\max} and the efficiency ratio $\mathcal{E}_{\max}/\mathcal{W}^M$ as a function of h_c for various values of M (see the legends). Panels (a-b) show the results for $h_i = 0.5$, whereas panels (c) and (d) illustrate those for $h_i = 1.5$. Insets: zoom in from $h_c = 0.3$ to 0.7. Numerically, we add a small offset 10^{-10} to \mathcal{W}^M to avoid undefined values when $h_c = h_i$.

The full time-dependent results of the ergotropy and work are shown in App. D for the different quenching strategies. From these data, we extract the maximum total ergotropy \mathcal{E}_{\max} that is reached after the quench and its ratio $\mathcal{E}_{\max}/\mathcal{W}^M$ with the corresponding amount of work. In Fig. 4(a,b), we show these quantities as a function of the charger magnetic field strength h_c starting in

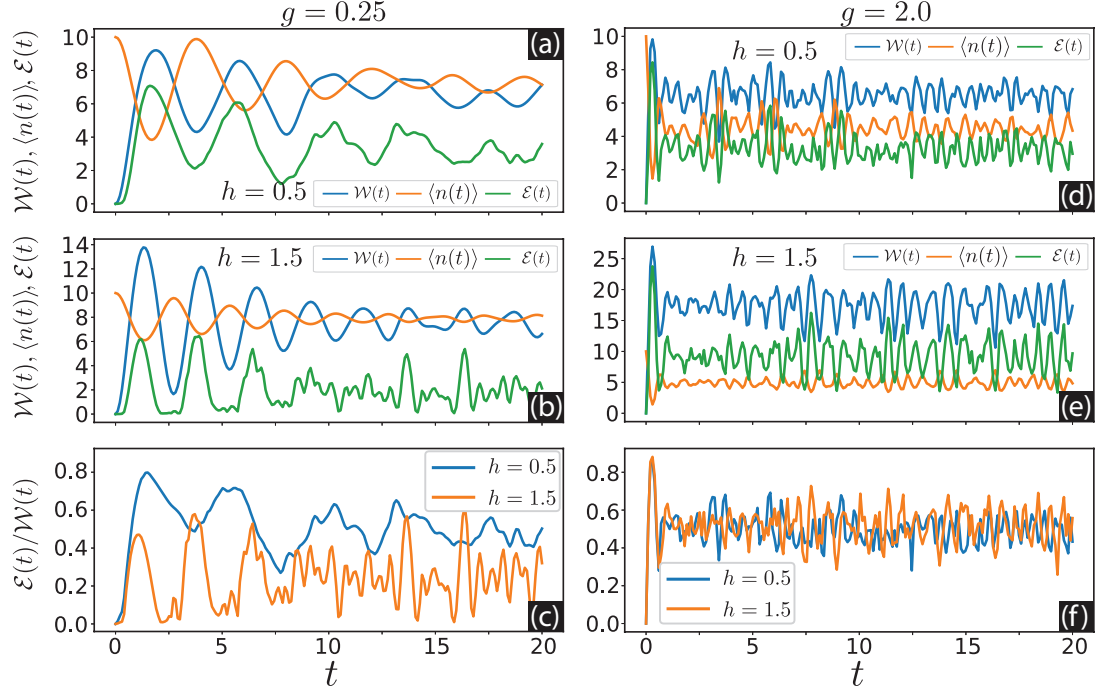


FIG. 5. Time evolution of the stored energy $\mathcal{W}(t)$, the average photon number $\langle n(t) \rangle$, the ergotropy $\mathcal{E}(t)$, and the ratio $\mathcal{E}(t)/\mathcal{W}(t)$, for two coupling strengths: $g = 0.25$ (left column) and $g = 2.0$ (right column).

the broken phase ($h_i = 0.5$). For $M = N$, $\mathcal{E}_{\max} = \mathcal{W}_{\max}^M$. As M decreases, \mathcal{E}_{\max} similarly decreases as expected, as less energy can be extracted from a smaller numbers of cells. Near the initial magnetic field strength, $h_c \approx h_i$, the efficiency ratio $\mathcal{E}_{\max}/\mathcal{W}^M$ is diminished as shown in Fig. 4(b). However, it increases when quenching to either side of h_i reaching values above 0.9, highlighting the robustness of the LMG battery against detrimental correlation effects.

For $h_i = 1.5$, similar results are depicted in Figs. 4(c,d). Quenching from the symmetric phase into the broken phase offers a clear advantage in terms of the ergotropy, while again the ratio takes large values $\mathcal{E}_{\max}/\mathcal{W}^M > 0.9$ for $h_c < 1$. However, when quenching within the symmetric phase, $h_c > 1$, although the ratio $\mathcal{E}_{\max}/\mathcal{W}^M$ can take large values, the ergotropy itself is always very small, as shown in Fig. 4(c), indicating that this scenario is less favorable for any meaningful energy storage and extraction.

Finally, we also note that in both cases at $h_c = h_i$, \mathcal{E}_{\max} remains nonzero for $M < N$ due to the inherent ergotropy in the M cell subsystem arising from the interactions with the remaining spins $N - M$ cells that are present in the charged state. As the passive state does not include this interaction energy it is therefore extracted from the subsystem even when no charging quench is applied, and contributes a minor increase in ergotropy for $h_c \neq h_i$ as also noted in Ref. [83].

B. Charging by coupling to a bosonic oscillator environment

In this section, we analyze the charging efficiency of the QB through coupling to a bosonic bath, as described in **II B 2**. Here, we fix $N = M = 10$ spins. The bath is initialized as a Fock state $|n\rangle$, with n photons (here we consider $n = N = 10$). The battery parameters are fixed with $\lambda = 1$, and full anisotropy $\gamma = 0$. We consider two values of the external magnetic field, $h = h_i = 0.5$ (broken phase) and $h = h_i = 1.5$ (symmetric phase) in the following analysis so as to only examine the role the bath plays in the charging process. For numerical calculations the Fock space is truncated to 50 states which is sufficiently large to avoid finite-size effects for initial photon numbers up to 10.

We first focus on the regime of small battery-bath coupling $g = 0.25$, and show the stored work $\mathcal{W}(t)$, average photon number $\langle n(t) \rangle$ and the ergotropy $\mathcal{E}(t)$, for $h = 0.5$ and $h = 1.5$ in Fig. 5(a) and Fig. 5(b) respectively. For both magnetic field strengths, the stored work and average photon number exhibit damped oscillations that are out of phase: initially, $\mathcal{W}(t)$ increases from zero while $\langle n(t) \rangle$ decreases from its initial value of $n = 10$. This behavior reflects the exchange of energy between the bath and the battery which is induced by the sudden interaction quench.

While qualitatively the charging process is similar for both $h = 0.5$ and $h = 1.5$, the amount of work that can actually be extracted via the ergotropy is quite different. Indeed, while more work is stored in the symmetric phase

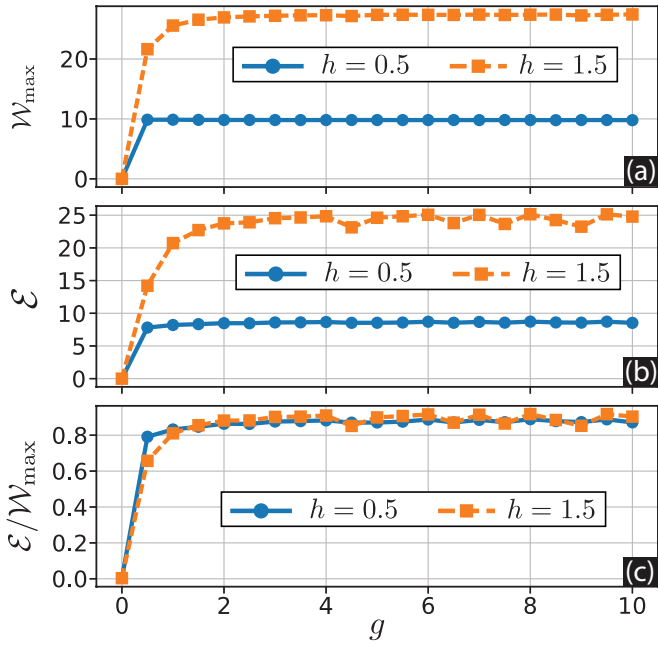


FIG. 6. (a) The maximum stored work W_{\max} , (b) the ergotropy \mathcal{E} at W_{\max} , and (c) the ratio \mathcal{E}/W_{\max} (c) as a function of coupling strength g for $h = 0.5$ (blue dotted line) and $h = 1.5$ (orange dotted line).

battery, the maximum ergotropy is actually comparable to the broken phase battery. Furthermore, the ergotropy can practically vanish in the symmetric phase battery when the stored work takes local minima at $t \approx 2.5$ and $t \approx 5$, while this is not the case for the broken phase battery. This difference in performance and energy transfer efficiency can be succinctly seen in the ratio $\mathcal{E}(t)/W(t)$ shown in Fig. 5(c), which shows that on average a larger amount of extractable work can be stored in the broken phase battery, and which crucially is more stable on longer times.

When the coupling between the battery and bath is large, $g = 2$, we again observe clear signatures of energy exchange between the battery and the bath, indicated by the reduction in the average photon number and subsequent increase in work and ergotropy (see Fig. 5(d,e)). For the broken phase battery, the long time behavior of the stored work and the ergotropy is equivalent to the weak coupling case (see Fig. 5(a)), albeit with faster oscillations caused by the increased battery-bath coupling. However, for the symmetric battery significantly more work is stored and ergotropy extracted, more than double in both cases, than in the same battery at weak coupling (see Fig. 5(b)). Furthermore, the ratio $\mathcal{E}(t)/W(t)$ is now equivalent for both broken phase and symmetric phase batteries, as shown in Fig. 5(f), indicating similar performance in terms of the percentage of energy that can be extracted.

While this implies that stronger coupling leads to more powerful batteries, we find that already at $g = 2$ the maximum performance is reached in this system. We

can see this in Fig. 6 where we show the the maximum stored work W_{\max} , ergotropy \mathcal{E} at W_{\max} , and their ratio as functions of the coupling strength g . For the broken phase battery, the maximum stored work and ergotropy have essentially saturated to a fixed value at $g = 0.5$, while for the symmetric battery this occurs around $g = 2$.

Comparing the maximum stored and extracted work of the two batteries we find that both W_{\max} and \mathcal{E} attain significantly higher values for the symmetric battery with $h = 1.5$. This behavior can be understood by examining the energy spectrum of the QB shown in Fig. 2(a). At $h = 0.5$, the system exhibits a nearly degenerate energy gap $\varepsilon_l - \varepsilon_0$, which limits the energy that can be stored. In contrast, at $h = 1.5$, the energy levels are non-degenerate and the energy gaps increase with h , thereby raising the upper bound of storables energy. This observation is consistent with earlier studies [23, 45], which demonstrated that the form of the energy spectrum plays a crucial role in determining the maximum stored energy in a QB. In our case, the field-dependent energy spectrum sets a natural upper limit for W_{\max} and \mathcal{E} . The observed saturation with increasing g indicates that this limit is eventually reached, and stronger coupling cannot further increase the battery's storage capacity.

To further support our results, we show in Fig. 7 the energy distribution $P(\varepsilon_j) = \langle \zeta(\varepsilon_j) | \rho_B | \zeta(\varepsilon_j) \rangle$ as a function of eigenvalues ε_j , where $\{|\zeta(\varepsilon_j)\rangle\}$ are eigenstates of H_B and ρ_B is the battery state after tracing out the bath. The shown results correspond to the same time that W_{\max} is reached.

Once the coupling g is turned on, energy begins to flow between the bath and the battery, causing the work to increase and the population to spread into higher energy levels with $\varepsilon_j > \varepsilon_0$. Since the interaction term in Eq. (3) does not commute with H_B , switching on the coupling between the QB and the bath injects irreversible work into the system. Consequently, the energy stored in the QB at the end of the charging process originates not only from the bath but also from the external work performed during charging. In particular, the broken phase battery already occupies higher energy eigenstates for $g = 0.25$, while the symmetric battery is normally distributed in the centre of the spectrum (see Fig. 7(a)). As the coupling becomes stronger, the population gradually shifts

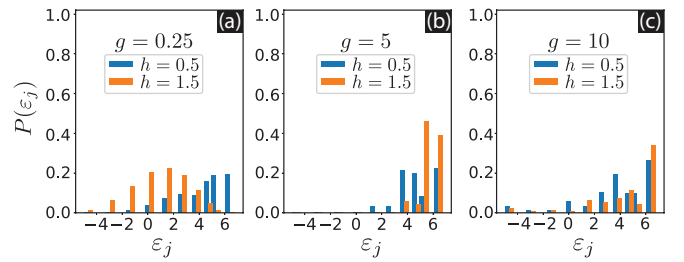


FIG. 7. Occupations $P(\varepsilon_j)$ of the eigenstates of battery Hamiltonian H_B as a function of the eigenenergies ε_j for battery-bath couplings (a) $g = 0.25$, (b) $g = 5$ and (c) $g = 10$.

upward through the energy ladder and eventually approaches the maximum level, $\varepsilon_{j_{\max}}$, as in Fig. 7(b). At $g = 10$, both batteries capacity saturates as levels close to $\varepsilon_{j_{\max}}$ are occupied as seen in Fig. 7(c). Complete population inversion of either battery is not reached due to irreversible excitations that are created during the coupling process, along with non-Markovian effects from strong coupling to the bath [84–87]. This results in lower energy eigenstates of the battery being occupied throughout the charging process leading to a reduction in extractable work as seen in the ergotropy in Fig. 6(c).

IV. CONCLUSION

In this paper, we have studied the performance of the LMG-based QB, which is charged by either quenching a magnetic field or coupling to a bosonic environment. We have shown that quenching a symmetric phase QB across the critical point results in the significant enhancement in the stored work, along with stable and efficient ergotropy extraction. If we charge the QB by strongly coupling to the bosonic bath, the symmetric phase QB shows a better performance compared to its broken symmetry counterpart due to its non-degenerated energy levels, while still maintaining the same work extraction ratio. These results highlight the magnetic field dynamics and environmental coupling as key factors in optimizing charging performance.

The study emphasizes that precise control over both the parameters for magnetic field quenching and the strength of the bosonic bath coupling is essential for achieving maximum energy storage efficiency. The LMG model's ability to maintain high ergotropy under these conditions underscores its potential as a robust framework for quantum energy storage.

In addition to demonstrating the advantages of this approach, our findings also pave the way for future investigations. Further research could focus on developing advanced optimization protocols to refine quenching strategies and coupling dynamics. Exploring other types of environmental couplings or extending this approach to multi-qubit quantum batteries could provide deeper insights and enhance the practical applicability of quantum energy storage technologies.

ACKNOWLEDGMENTS

This research was supported by the SHINKA grant at the Okinawa Institute of Science and Technology (OIST) and was also conducted while visiting the OIST through the Theoretical Sciences Visiting Program (TSVP). T.B., T.F., and T.D.A.-T. thank support from JST COI-NEXT Grant No. JPMJPF2221. T.F. is also grateful to JSPS KAKENHI Grant No. JP23K03290. T.D.A.-T. acknowledges support through a Dodge Postdoctoral Researcher Fellowship at the University of Oklahoma.

DATA AVAILABILITY

The data that support the findings of this article are openly available [88].

CONFLICT OF INTEREST

The authors declare that there are no conflicts of interest associated with this study.

Appendix A: The spectral decomposition of the LMG Hamiltonian

To numerically obtain the complete spectrum of the Lipkin-Meshkov-Glick (LMG) model described by the Hamiltonian

$$H_{\text{LMG}} = \frac{\lambda}{N} \sum_{i < j}^N (\sigma_x^i \sigma_x^j + \gamma \sigma_y^i \sigma_y^j) + h \sum_{i=1}^N \sigma_z^i, \quad (\text{A.1})$$

it is natural to employ the Dicke basis since the matrix elements can be computed analytically within this framework (see Refs. [58, 89, 90] for further details). In doing so, we will use the angular momentum operators J_α defined as

$$J_\alpha = \frac{1}{2} \sum_{i=1}^N \sigma_\alpha^i, \quad (\text{A.2})$$

where σ_α with $\alpha = x, y, z$ denotes the Pauli matrices. Straightforwardly, the Zeeman term simply becomes

$$h \sum_i \sigma_z^i = 2hJ_z. \quad (\text{A.3})$$

Let us then rewrite the two-body term $\sum_{i < j} \sigma_\alpha^i \sigma_\alpha^j$ in Eq.(A.1) in terms of the operator J_α using the expression

$$\left(\sum_{i=1}^N \sigma_\alpha^i \right)^2 = \sum_{i=1}^N (\sigma_\alpha^i)^2 + 2 \sum_{i < j} \sigma_\alpha^i \sigma_\alpha^j. \quad (\text{A.4})$$

It is apparent that for the i -th particle we have $(\sigma_\alpha^i)^2 = \mathbb{I}$, yielding

$$\sum_{i=1}^N (\sigma_\alpha^i)^2 = N\mathbb{I}, \quad (\text{A.5})$$

with \mathbb{I} being the identity matrix. Hence, we get

$$\sum_{i < j} \sigma_\alpha^i \sigma_\alpha^j = \frac{1}{2} \left[\left(\sum_{i=1}^N \sigma_\alpha^i \right)^2 - N\mathbb{I} \right]. \quad (\text{A.6})$$

Plugging Eq. (A.2) into Eq. (A.6) yields

$$\sum_{i < j} \sigma_\alpha^i \sigma_\alpha^j = \frac{1}{2} (4J_\alpha^2 - N\mathbb{I}) = 2J_\alpha^2 - \frac{N}{2}\mathbb{I}. \quad (\text{A.7})$$

Explicitly, we obtain

$$\sum_{i < j} (\sigma_x^i \sigma_x^j + \gamma \sigma_y^i \sigma_y^j) = 2 (J_x^2 + \gamma J_y^2) - \frac{N}{2} (1 + \gamma) \mathbb{I}. \quad (\text{A.8})$$

The Hamiltonian (A.1) is then transformed into

$$H_{\text{LMG}} = \frac{2\lambda}{N} (J_x^2 + \gamma J_y^2) + 2hJ_z - \frac{\lambda}{2} (1 + \gamma) \mathbb{I}. \quad (\text{A.9})$$

It is clear that the term proportional to \mathbb{I} uniformly shifts the entire spectrum by $-0.5\lambda(1 + \gamma)$, thereby not influencing neither the eigenstates nor energy differences. Consequently, it is safe and customary to exclude it from Eq. (A.9) for the sake of simplicity.

Afterward, we employ the Dicke basis $|j, m\rangle$, where j is the total angular momentum quantum number and m is the magnetic quantum number ranging from $-j$ to j . For N spin-1/2 particles, it is noted that the total angular momentum quantum number j can take values $0, 1/2, 1, \dots, N/2$, however we only focus on the maximum angular momentum quantum number $j_{\text{max}} = N/2$ due to the permutation invariance of the collective spin system [54], ie., the total angular momentum \mathbf{J} is conserved, $[\mathbf{J}, H_{\text{LMG}}] = 0$. This leads to a Hilbert space of dimension $d = N + 1$. For simplicity, we will write $|j_{\text{max}} = N/2, m\rangle$ by $|m\rangle$ throughout the remaining of this appendix. To further simplify calculations, it is convenient to rewrite the operators J_x , and J_y in terms of the collective spin raising and lowering operators (also known as the ladder operators) J_+ , and J_- , which are defined as

$$J_x = \frac{1}{2} (J_+ + J_-), \text{ and } J_y = \frac{1}{2i} (J_+ - J_-). \quad (\text{A.10})$$

In the Dicke basis, the eigenvalues and eigenstates of the

operators J_z , J_+ , and J_- are respectively given as

$$J_z|m\rangle = m|m\rangle, \quad (\text{A.11})$$

$$J_+|m\rangle = \sqrt{(N/2 - m)(N/2 + m + 1)}|m + 1\rangle, \quad (\text{A.12})$$

$$J_-|m\rangle = \sqrt{(N/2 + m)(N/2 - m + 1)}|m - 1\rangle, \quad (\text{A.13})$$

$$J_+ J_-|m\rangle = (N/2 + m)(N/2 - m + 1)|m\rangle, \quad (\text{A.14})$$

$$J_- J_+|m\rangle = (N/2 - m)(N/2 + m + 1)|m\rangle, \quad (\text{A.15})$$

$$J_\pm^2|m\rangle = \sqrt{(A_\pm + N)(A_\pm - 1)}|m \pm 2\rangle, \quad (\text{A.16})$$

where $A_\pm = N^2/4 - m^2 \mp 2m$.

With the use of the Dicke basis and the angular momentum operators J_α , the matrix representation of the Hamiltonian (A.9) has the banded form as follow:

$$\begin{aligned} H_{m'm} &= \langle m'|H|m\rangle \\ &= \frac{\lambda}{2N} (1 + \gamma) \sqrt{(A_- + N)(A_- - 1)} \delta_{m',m-2} \\ &\quad + \left[2mh + \frac{\lambda}{2N} (1 + \gamma) (N(0.5N + 1) - 2m^2) \right] \delta_{m',m} \\ &\quad + \frac{\lambda}{2N} (1 + \gamma) \sqrt{(A_+ + N)(A_+ - 1)} \delta_{m',m+2}. \end{aligned} \quad (\text{A.17})$$

We remark that the $(N + 1) \times (N + 1)$ matrix representing the LMG Hamiltonian in the Dicke basis can then be numerically diagonalized to obtain the eigenvalues and eigenstates by using well-known linear algebra packages or computational software. Specifically, we used the function ‘eigsh’ implemented in the SciPy library for the matrix diagonalization in this work.

Appendix B: The isotropic LMG-based battery

In the following appendix, we consider the LMG-based battery in the isotropic case, $\gamma = 1$, and demonstrate that this case is not a good candidate for realizing QBs. In the isotropic case, the LMG Hamiltonian is given by

$$\begin{aligned} H &= \frac{2}{N} (J_x^2 + J_y^2) + 2hJ_z \\ &= \frac{2}{N} (\mathbf{J}^2 - J_z^2) + 2hJ_z, \end{aligned} \quad (\text{B.1})$$

where $\mathbf{J}^2 = J_x^2 + J_y^2 + J_z^2$. It can be seen that this Hamiltonian is already diagonal in the Dicke basis $|m\rangle$, where $-N/2 \leq m \leq N/2$. Consequently, in this situation the eigenstates of the LMG Hamiltonian $|\varepsilon_l\rangle = |N/2 - l\rangle$ are exactly the Dicke basis $|m\rangle$, and the corresponding eigenvalues are

$$\varepsilon_l = \begin{cases} -\frac{2}{N} \left(\left[\frac{Nh}{2} \right] - \frac{l}{2} - \frac{Nh}{2} \right)^2 + \left(\frac{Nh^2}{2} + \frac{N}{2} + 1 \right) & \text{for } 0 \leq h < 1, \\ -\frac{2}{N} \left(\frac{N}{2} - l - \frac{Nh}{2} \right)^2 + \left(\frac{Nh^2}{2} + \frac{N}{2} + 1 \right) & \text{for } h > 1, \end{cases} \quad (\text{B.2})$$

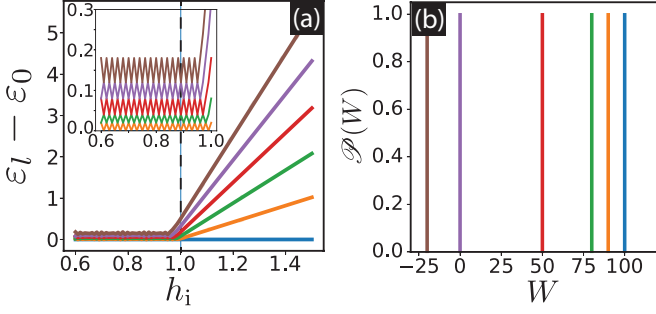


FIG. 8. (a) Energy gap between the ground state and the first five excited states as a function of h_i for $N = 100$ and $\gamma = 1$. (b) Work probability distribution $\mathcal{P}(W)$ for different h_i from right to left: 0.0, 0.1, 0.2, 0.5, 1, 1.2.

where $[x]$ denotes the standard rounding function [57]. As a result, the energy gap $\varepsilon_l - \varepsilon_0$ yields

$$\varepsilon_l - \varepsilon_0 = \begin{cases} \frac{4l}{N} \left(\frac{Nh}{2} - \left[\frac{Nh}{2} \right] + \frac{l}{2} \right) - \frac{2}{N} l^2 & \text{for } 0 \leq h < 1, \\ 2l(h-1) - \frac{2}{N} l^2 & \text{for } h > 1, \end{cases} \quad (\text{B.3})$$

and closes at $h = (2p + l)/N$ between the two states $|\varepsilon_l\rangle = |m = N/2 - l + 1\rangle$ and $|\varepsilon_l\rangle = |m = N/2 - l\rangle$, for $p \leq 0$ is an integer and $l \geq 1$. Fig. 8(a) illustrates the energy gap for the isotropic case.

We also analyze the work distribution $\mathcal{P}(W)$, shown in Fig. 8(b), with $|\varepsilon_l\rangle = |\mu_l\rangle = |N/2 - l\rangle$. In this case, $\langle \mu_k | \varepsilon_0 \rangle \langle \varepsilon_l | \mu_k \rangle = 0$ for all $l > 0$ and k . As a result, $\mathcal{P}(W) = 1$ for all h_c , leading to $\mathcal{W}(t) = 0$ at all times. This indicates that the energy remains unchanged, meaning that the isotropic LMG model is not a suitable candidate for realizing QBs.

Appendix C: Average of the extracted energy in the sudden quench

The long-time averaged work $\langle \mathcal{W} \rangle$ is defined as

$$\langle \mathcal{W} \rangle = \lim_{T \rightarrow \infty} \frac{1}{T} \int_0^T \mathcal{W}(t) dt = \sum_l \langle \mathcal{P}_l(t) \rangle (\varepsilon_l - \varepsilon_0). \quad (\text{C.1})$$

where the long-time averaged population is given by

$$\begin{aligned} \langle \mathcal{P}_l(t) \rangle &= \lim_{T \rightarrow \infty} \frac{1}{T} \int_0^T \mathcal{P}_l(t) dt \\ &= \lim_{T \rightarrow \infty} \frac{1}{T} \int_0^T dt \left[\sum_{k, k'} e^{-i(\mu_k - \mu_{k'})t} \langle \mu_k | \varepsilon_0 \rangle \langle \varepsilon_l | \mu_k \rangle \langle \mu_{k'} | \varepsilon_0 \rangle^* \langle \varepsilon_l | \mu_{k'} \rangle^* \right]. \end{aligned} \quad (\text{C.2})$$

After some basic algebraic calculations, we obtain

$$\langle \mathcal{P}_l(t) \rangle = \sum_k |\langle \mu_k | \varepsilon_0 \rangle|^2 |\langle \varepsilon_l | \mu_k \rangle|^2, \quad (\text{C.3})$$

where the off-diagonal elements with $k \neq k'$ vanish over the long-time average due to oscillatory integration. Substituting Eq. (C.3) into Eq. (C.1) yields

$$\langle \mathcal{W} \rangle = \sum_l \sum_k |\langle \mu_k | \varepsilon_0 \rangle|^2 |\langle \varepsilon_l | \mu_k \rangle|^2 (\varepsilon_l - \varepsilon_0). \quad (\text{C.4})$$

The variance of the total work $\mathcal{W}(t)$ over the long-time dynamics is defined as

$$\text{Var}(\mathcal{W}) = \langle \mathcal{W}^2 \rangle - \langle \mathcal{W} \rangle^2, \quad (\text{C.5})$$

where

$$\begin{aligned} \langle \mathcal{W}^2 \rangle &= \sum_{l, l'} \langle \mathcal{P}_l(t) \mathcal{P}_{l'}(t) \rangle (\varepsilon_l - \varepsilon_0)(\varepsilon_{l'} - \varepsilon_0) \\ &= \sum_{l, l'} \sum_k |\langle \mu_k | \varepsilon_0 \rangle|^2 |\langle \varepsilon_l | \mu_k \rangle|^2 \times \\ &\quad |\langle \varepsilon_{l'} | \mu_k \rangle|^2 (\varepsilon_l - \varepsilon_0)(\varepsilon_{l'} - \varepsilon_0). \end{aligned} \quad (\text{C.6})$$

Explicitly, the variance of the total work over the long-time dynamics is given as

$$\begin{aligned} \text{Var}(\mathcal{W}) &= \sum_{l, l'} \sum_k |\langle \mu_k | \varepsilon_0 \rangle|^2 |\langle \varepsilon_l | \mu_k \rangle|^2 |\langle \varepsilon_{l'} | \mu_k \rangle|^2 \times \\ &\quad (\varepsilon_l - \varepsilon_0)(\varepsilon_{l'} - \varepsilon_0) \\ &\quad - \left[\sum_l \sum_k |\langle \mu_k | \varepsilon_0 \rangle|^2 |\langle \varepsilon_l | \mu_k \rangle|^2 (\varepsilon_l - \varepsilon_0) \right]^2, \end{aligned} \quad (\text{C.7})$$

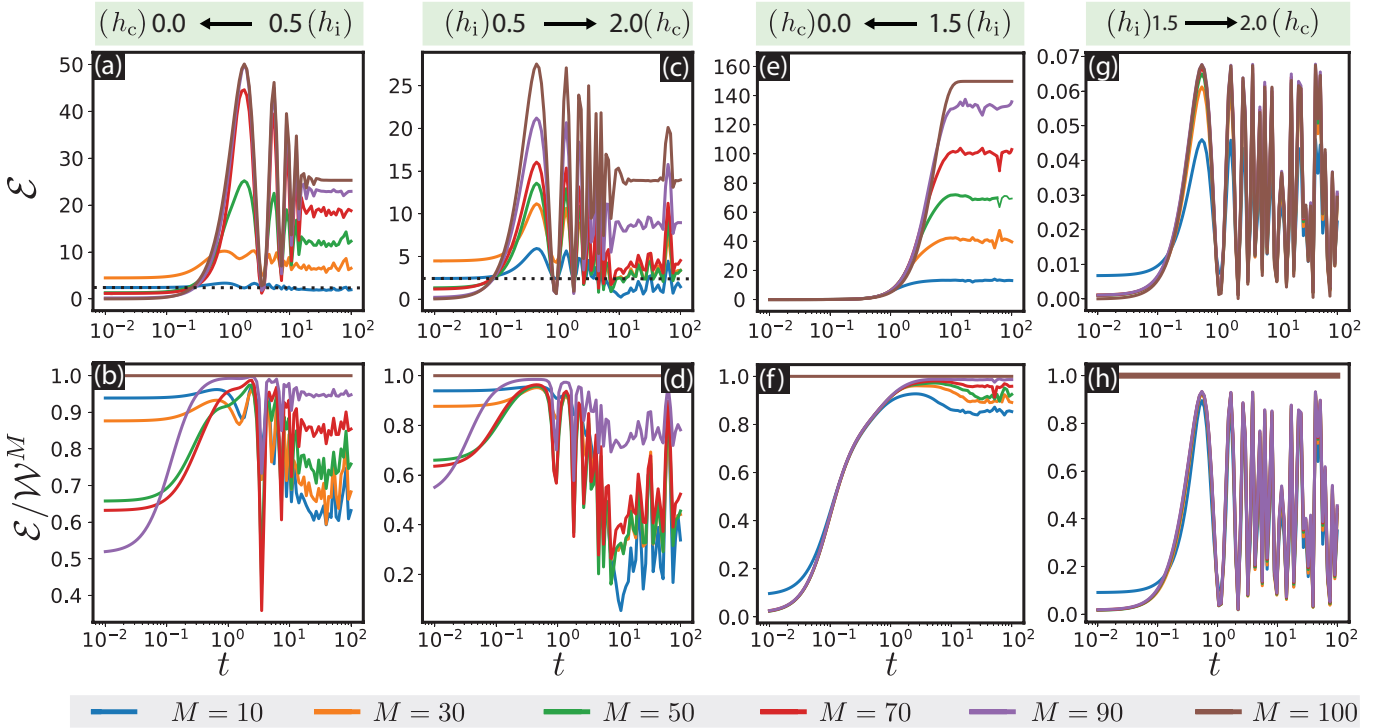


FIG. 9. The time evolution of the ergotropy \mathcal{E} and the efficiency ratio $\mathcal{E}/\mathcal{W}^M$ for different quenching protocols.

Appendix D: Time-dependent of the extracted energy in the sudden quench

This section presents the time evolution of the extracted energy via ergotropy \mathcal{E} and the efficiency ratio \mathcal{E}/\mathcal{W} , where \mathcal{E} and \mathcal{W} are defined in Eqs. (11, 13) in the main text. The results, shown in Fig. 9, correspond to different quenching protocols:

- (a,b): Quenching within the broken phase from $h_i = 0.5$ to $h_c = 0.0$.
- (c,d): Quenching from the broken phase to the

symmetric phase, $h_i = 0.5$ to $h_c = 2.0$.

- (e,f): Quenching from the symmetric phase to the broken phase, $h_i = 1.5$ to $h_c = 0.0$.
- (g,h): Quenching within the symmetric phase from $h_i = 1.5$ to $h_c = 2.0$.

The third case is the most effective charging protocol, while the last case is the least effective. We also emphasize that the relative ergotropy, the extractable energy after the quench compared to the initial state, can become negative at longer times. For example, in Figs. 9(a, c) for $M = 10$, the relative ergotropy turns negative around $t = 10$, as indicated by the data going below the dotted black line.

[1] F. Campaioli, S. Gherardini, J. Q. Quach, M. Polini, and G. M. Andolina, Colloquium: Quantum batteries, *Rev. Mod. Phys.* **96**, 031001 (2024).

[2] F. Binder, L. A. Correa, C. Gogolin, J. Anders, and G. Adesso, eds., *Thermodynamics in the Quantum Regime: Fundamental Aspects* 1st ed., Fundamental Theories of Physics, Vol. 195 (Springer Cham, 2019) pp. XII, 998, 435 b/w illustrations, 189 illustrations in colour.

[3] F. Pirmoradian and K. Mølmer, Aging of a quantum battery, *Phys. Rev. A* **100**, 043833 (2019).

[4] D. Ferraro, M. Campisi, G. M. Andolina, V. Pellegrini, and M. Polini, High-power collective charging of a solid-state quantum battery, *Phys. Rev. Lett.* **120**, 117702 (2018).

[5] A. Crescente, M. Carrega, M. Sassetti, and D. Ferraro, Ultrafast charging in a two-photon dicke quantum battery, *Phys. Rev. B* **102**, 245407 (2020).

[6] S. Gherardini, M. Andolina, M. Keck, A. Mari, V. Giovannetti, and M. Polini, Quantum versus classical many-body batteries, *Phys. Rev. B* **99**, 205437 (2019).

[7] F. C. Binder, S. Vinjanampathy, K. Modi, and J. Goold, Quantacell: powerful charging of quantum batteries, *New Journal of Physics* **17**, 075015 (2015).

[8] F.-Q. Dou, Y.-Q. Lu, Y.-J. Wang, and J.-A. Sun, Extended dicke quantum battery

with interatomic interactions and driving field, *Phys. Rev. B* **105**, 115405 (2022).

[9] D. Rosa, D. Rossini, G. M. Andolina, M. Polini, and M. Carrega, Ultra-stable charging of fast-scrambling syk quantum batteries, *Journal of High Energy Physics* **2020**, 67 (2020).

[10] D. Rossini, G. M. Andolina, D. Rosa, M. Carrega, and M. Polini, Quantum advantage in the charging process of sachdev-ye-kitaev batteries, *Phys. Rev. Lett.* **125**, 236402 (2020).

[11] D.-L. Yang, F.-M. Yang, and F.-Q. Dou, Three-level dicke quantum battery, *Phys. Rev. B* **109**, 235432 (2024).

[12] T. P. Le, J. Levinsen, K. Modi, M. M. Parish, and F. A. Pollock, Spin-chain model of a many-body quantum battery, *Phys. Rev. A* **97**, 022106 (2018).

[13] F. Zhao, F.-Q. Dou, and Q. Zhao, Quantum battery of interacting spins with environmental noise, *Phys. Rev. A* **103**, 033715 (2021).

[14] F. Zhao, F.-Q. Dou, and Q. Zhao, Charging performance of the su-schrieffer-heeger quantum battery, *Phys. Rev. Res.* **4**, 013172 (2022).

[15] F. Barra, K. V. Hovhannisan, and A. Imparato, Quantum batteries at the verge of a phase transition, *New Journal of Physics* **24**, 015003 (2022).

[16] F.-Q. Dou, H. Zhou, and J.-A. Sun, Cavity heisenberg-spin-chain quantum battery, *Phys. Rev. A* **106**, 032212 (2022).

[17] Y. Huangfu and J. Jing, High-capacity and high-power collective charging with spin chargers, *Phys. Rev. E* **104**, 024129 (2021).

[18] D. Rossini, G. M. Andolina, and M. Polini, Many-body localized quantum batteries, *Phys. Rev. B* **100**, 115142 (2019).

[19] S. Ghosh, T. Chanda, and A. Sen(De), Enhancement in the performance of a quantum battery by ordered and disordered interactions, *Phys. Rev. A* **101**, 032115 (2020).

[20] M. Carrega, A. Crescente, D. Ferraro, and M. Sasetti, Dissipative dynamics of an open quantum battery, *New Journal of Physics* **22**, 083085 (2020).

[21] J. Q. Quach and W. J. Munro, Using dark states to charge and stabilize open quantum batteries, *Phys. Rev. Appl.* **14**, 024092 (2020).

[22] S. Ghosh and A. Sen(De), Dimensional enhancements in a quantum battery with imperfections, *Phys. Rev. A* **105**, 022628 (2022).

[23] L. Peng, W.-B. He, S. Chesi, H.-Q. Lin, and X.-W. Guan, Lower and upper bounds of quantum battery power in multiple central spin systems, *Phys. Rev. A* **103**, 052220 (2021).

[24] F. Caravelli, B. Yan, L. P. García-Pintos, and A. Hamma, Energy storage and coherence in closed and open quantum batteries, *Quantum* **5**, 505 (2021).

[25] J.-X. Liu, H.-L. Shi, Y.-H. Shi, X.-H. Wang, and W.-L. Yang, Entanglement and work extraction in the central-spin quantum battery, *Phys. Rev. B* **104**, 245418 (2021).

[26] M. B. Arjmandi, H. Mohammadi, and A. C. Santos, Enhancing self-discharging process with disordered quantum batteries, *Phys. Rev. E* **105**, 054115 (2022).

[27] S. Mondal and S. Bhattacharjee, Periodically driven many-body quantum battery, *Phys. Rev. E* **105**, 044125 (2022).

[28] M. B. Arjmandi, H. Mohammadi, A. Saguia, M. S. Sarandy, and A. C. Santos, Localiza-

tion effects in disordered quantum batteries, *Phys. Rev. E* **108**, 064106 (2023).

[29] D. T. Hoang, F. Metz, A. Thomasen, T. D. Anh-Tai, T. Busch, and T. Fogarty, Variational quantum algorithm for ergotropy estimation in quantum many-body batteries, *Phys. Rev. Res.* **6**, 013038 (2024).

[30] A. Catalano, S. Giampaolo, O. Morsch, V. Giovannetti, and F. Franchini, Frustrating quantum batteries, *PRX Quantum* **5**, 030319 (2024).

[31] A. C. Santos, A. Saguia, and M. S. Sarandy, Stable and charge-switchable quantum batteries, *Phys. Rev. E* **101**, 062114 (2020).

[32] F. Campaioli, F. A. Pollock, F. C. Binder, L. Céleri, J. Goold, S. Vinjanampathy, and K. Modi, Enhancing the charging power of quantum batteries, *Phys. Rev. Lett.* **118**, 150601 (2017).

[33] F. H. Kamin, F. T. Tabesh, S. Salimi, and A. C. Santos, Entanglement, coherence, and charging process of quantum batteries, *Phys. Rev. E* **102**, 052109 (2020).

[34] T. K. Konar, L. G. C. Lakkaraju, and A. Sen (De), Quantum battery with non-hermitian charging, *Phys. Rev. A* **109**, 042207 (2024).

[35] R. Shastri, C. Jiang, G.-H. Xu, B. Prasanna Venkatesh, and G. Watanabe, Dephasing enabled fast charging of quantum batteries, *npj Quantum Information* **11**, 9 (2025).

[36] S. Ghosh, T. Chanda, S. Mal, and A. Sen(De), Fast charging of a quantum battery assisted by noise, *Phys. Rev. A* **104**, 032207 (2021).

[37] R. R. Rodriguez, B. Ahmadi, G. Suárez, P. Mazurek, S. Barzanjeh, and P. Horodecki, Optimal quantum control of charging quantum batteries, *New Journal of Physics* **26**, 043004 (2024).

[38] P. A. Erdman, G. M. Andolina, V. Giovannetti, and F. Noé, Reinforcement learning optimization of the charging of a dicke quantum battery, *Phys. Rev. Lett.* **133**, 243602 (2024).

[39] F. Mazzoncini, V. Cavina, G. M. Andolina, P. A. Erdman, and V. Giovannetti, Optimal control methods for quantum batteries, *Phys. Rev. A* **107**, 032218 (2023).

[40] V. T. Hai, V. Minh Kiet, L. V. Trung Duong, P. Hoai Luan, L. B. Ho, and Y. Nakashima, Quantum battery optimization through quantum machine learning techniques, in *2024 21st International SoC Design Conference (ISOCC)* (2024) pp. 121–122.

[41] Z. Belén, M. F. Santos, and F. Barra, Laser powered dissipative quantum batteries in atom-cavity qed, *New Journal of Physics* **26**, 073049 (2024).

[42] M. Hadipour, S. Haseli, D. Wang, and S. Haddadi, Proposed scheme for a cavity-based quantum battery, *Advanced Quantum Technologies* **7**, 2400115 (2024), <https://onlinelibrary.wiley.com/doi/pdf/10.1002/qute.202400115>.

[43] R. Salvia, M. Perarnau-Llobet, G. Haack, N. Brunner, and S. Nimmrichter, Quantum advantage in charging cavity and spin batteries by repeated interactions, *Phys. Rev. Res.* **5**, 013155 (2023).

[44] B. Ahmadi, P. Mazurek, P. Horodecki, and S. Barzanjeh, Nonreciprocal quantum batteries, *Phys. Rev. Lett.* **132**, 210402 (2024).

[45] S. Julià-Farré, T. Salamon, A. Riera, M. N. Bera, and M. Lewenstein, Bounds on the capacity and power of quantum batteries, *Phys. Rev. Res.* **2**, 023113 (2020).

[46] A. Bhattacharyya, K. Sen, and U. Sen, Non-

completely positive quantum maps enable efficient local energy extraction in batteries, *Phys. Rev. Lett.* **132**, 240401 (2024).

[47] G. Zhu, Y. Chen, Y. Hasegawa, and P. Xue, Charging quantum batteries via indefinite causal order: Theory and experiment, *Phys. Rev. Lett.* **131**, 240401 (2023).

[48] Z.-G. Lu, G. Tian, X.-Y. Lü, and C. Shang, *Topological quantum batteries* (2024), arXiv:2405.03675 [quant-ph].

[49] X. Yang, Y.-H. Yang, X.-Z. Liu, J.-L. Jiang, X.-Z. Zheng, S.-M. Fei, and M.-X. Luo, Experimental verification of quantum battery capacity with an optical platform, *Cell Reports Physical Science* **5**, 102300 (2024).

[50] D. Qu, X. Zhan, H. Lin, and P. Xue, Experimental optimization of charging quantum batteries through a catalyst system, *Phys. Rev. B* **108**, L180301 (2023).

[51] H. Lipkin, N. Meshkov, and A. Glick, Validity of many-body approximation methods for a solvable model: (i). exact solutions and perturbation theory, *Nuclear Physics* **62**, 188 (1965).

[52] N. Meshkov, A. Glick, and H. Lipkin, Validity of many-body approximation methods for a solvable model: (ii). linearization procedures, *Nuclear Physics* **62**, 199 (1965).

[53] A. Glick, H. Lipkin, and N. Meshkov, Validity of many-body approximation methods for a solvable model: (iii). diagram summations, *Nuclear Physics* **62**, 211 (1965).

[54] B. A. Chase and J. M. Geremia, Collective processes of an ensemble of spin-1/2 particles, *Phys. Rev. A* **78**, 052101 (2008).

[55] J. Ma and X. Wang, Fisher information and spin squeezing in the lipkin-meshkov-glick model, *Phys. Rev. A* **80**, 012318 (2009).

[56] R. Botet, R. Jullien, and P. Pfeuty, Size scaling for infinitely coordinated systems, *Phys. Rev. Lett.* **49**, 478 (1982).

[57] S. Dusuel and J. Vidal, Continuous unitary transformations and finite-size scaling exponents in the lipkin-meshkov-glick model, *Phys. Rev. B* **71**, 224420 (2005).

[58] S. Campbell, Criticality revealed through quench dynamics in the lipkin-meshkov-glick model, *Phys. Rev. B* **94**, 184403 (2016).

[59] P. Ribeiro, J. Vidal, and R. Mosseri, Thermodynamical limit of the lipkin-meshkov-glick model, *Phys. Rev. Lett.* **99**, 050402 (2007).

[60] P. Ribeiro, J. Vidal, and R. Mosseri, Exact spectrum of the lipkin-meshkov-glick model in the thermodynamic limit and finite-size corrections, *Phys. Rev. E* **78**, 021106 (2008).

[61] R. Botet and R. Jullien, Large-size critical behavior of infinitely coordinated systems, *Phys. Rev. B* **28**, 3955 (1983).

[62] H. Morita, H. Ohnishi, J. da Providência, and S. Nishiyama, Exact solutions for the lmg model hamiltonian based on the bethe ansatz, *Nuclear Physics B* **737**, 337 (2006).

[63] F. Pan and J. Draayer, Analytical solutions for the lmg model, *Physics Letters B* **451**, 1 (1999).

[64] G. Ortiz, R. Somma, J. Dukelsky, and S. Rombouts, Exactly-solvable models derived from a generalized gaudin algebra, *Nuclear Physics B* **707**, 421 (2005).

[65] S. Dusuel and J. Vidal, Finite-size scaling exponents of the lipkin-meshkov-glick model, *Phys. Rev. Lett.* **93**, 237204 (2004).

[66] T. Holstein and H. Primakoff, Field dependence of the intrinsic domain magnetization of a ferromagnet, *Phys. Rev.* **58**, 1098 (1940).

[67] H.-M. Kwok, W.-Q. Ning, S.-J. Gu, and H.-Q. Lin, Quantum criticality of the lipkin-meshkov-glick model in terms of fidelity susceptibility, *Phys. Rev. E* **78**, 032103 (2008).

[68] J. Ma, L. Xu, H.-N. Xiong, and X. Wang, Reduced fidelity susceptibility and its finite-size scaling behaviors in the lipkin-meshkov-glick model, *Phys. Rev. E* **78**, 051126 (2008).

[69] G. Salvatori, A. Mandarino, and M. G. A. Paris, Quantum metrology in lipkin-meshkov-glick critical systems, *Phys. Rev. A* **90**, 022111 (2014).

[70] L. Garbe, O. Abah, S. Felicetti, and R. Puebla, Critical quantum metrology with fully-connected models: from heisenberg to kibble-zurek scaling, *Quantum Science and Technology* **7**, 035010 (2022).

[71] V. Montenegro, C. Mukhopadhyay, R. Yousefjani, S. Sarkar, U. Mishra, M. G. A. Paris, and A. Bayat, *Review: Quantum metrology and sensing with many-body systems* (2024), arXiv:2408.15323 [quant-ph].

[72] T. Fogarty, S. Deffner, T. Busch, and S. Campbell, Orthogonality catastrophe as a consequence of the quantum speed limit, *Phys. Rev. Lett.* **124**, 110601 (2020).

[73] F.-Q. Dou, Y.-J. Wang, and J.-A. Sun, *Charging advantages of lipkin-meshkov-glick quantum battery* (2022), arXiv:2208.04831 [quant-ph].

[74] R. Islam, E. E. Edwards, K. Kim, S. Korenblit, C. Noh, H. Carmichael, G.-D. Lin, L.-M. Duan, C.-C. Joseph Wang, J. K. Freericks, and C. Monroe, Onset of a quantum phase transition with a trapped ion quantum simulator, *Nature Communications* **2**, 377 (2011).

[75] P. Richerme, Z.-X. Gong, A. Lee, C. Senko, J. Smith, M. Foss-Feig, S. Michalakis, A. V. Gorshkov, and C. Monroe, Non-local propagation of correlations in quantum systems with long-range interactions, *Nature* **511**, 198 (2014).

[76] P. Jurcevic, H. Shen, P. Hauke, C. Maier, T. Brydges, C. Hempel, B. P. Lanyon, M. Heyl, R. Blatt, and C. F. Roos, Direct observation of dynamical quantum phase transitions in an interacting many-body system, *Phys. Rev. Lett.* **119**, 080501 (2017).

[77] J. Zhang, G. Pagano, P. W. Hess, A. Kyprianidis, P. Becker, H. Kaplan, A. V. Gorshkov, Z.-X. Gong, and C. Monroe, Observation of a many-body dynamical phase transition with a 53-qubit quantum simulator, *Nature* **551**, 601 (2017).

[78] T. Zibold, E. Nicklas, C. Gross, and M. K. Oberthaler, Classical bifurcation at the transition from rabi to josephson dynamics, *Phys. Rev. Lett.* **105**, 204101 (2010).

[79] T. M. Hoang, M. Anquez, B. A. Robbins, X. Y. Yang, B. J. Land, C. D. Hamley, and M. S. Chapman, Parametric excitation and squeezing in a many-body spinor condensate, *Nature Communications* **7**, 11233 (2016).

[80] M. Anquez, B. A. Robbins, H. M. Bharath, M. Boguslawski, T. M. Hoang, and M. S. Chapman, Quantum kibble-zurek mechanism in a spin-1 bose-einstein condensate, *Phys. Rev. Lett.* **116**, 155301 (2016).

[81] M. Campisi, P. Hänggi, and P. Talkner, Colloquium: Quantum fluctuation relations: Foundations and applications, *Reviews of Modern Physics* **83**, 771 (2011).

[82] C. Campbell, T. Fogarty, and T. Busch, Nonequilibrium many-body dynamics in supersymmetric quenching,

Phys. Rev. Res. **4**, 033014 (2022).

[83] B. n. Mula, E. M. Fernández, J. E. Alvarellos, J. J. Fernández, D. García-Aldea, S. N. Santalla, and J. Rodríguez-Laguna, Ergotropy and entanglement in critical spin chains, *Phys. Rev. B* **107**, 075116 (2023).

[84] S.-C. Zhao, L. Luo, and N.-Y. Zhuang, *Stabilizing ergotropy in spin-chain quantum batteries via energy-invariant symmetry breaking: strengthen and bosonic cobathing* (2025), arXiv:2508.02772 [quant-ph].

[85] F. H. Kamin, F. T. Tabesh, S. Salimi, F. Kheirandish, and A. C. Santos, Non-markovian effects on charging and self-discharging process of quantum batteries, *New Journal of Physics* **22**, 083007 (2020).

[86] F. Barra, Efficiency fluctuations in a quantum battery charged by a repeated interaction process, *Entropy* **24**, 10.3390/e24060820 (2022).

[87] H.-L. Shi, S. Ding, Q.-K. Wan, X.-H. Wang, and W.-L. Yang, Entanglement, coherence, and extractable work in quantum batteries, *Phys. Rev. Lett.* **129**, 130602 (2022).

[88] L. B. Ho, D. T. Hoang, T. D. Anh-Tai, T. Busch, and T. Fogarty, Supporting data for boosting the performance of a lipkin-meshkov-glick quantum battery *in asymmetrically breaking strengths and bosonic cobathing* https://github.com/echkon/lmg_quantum_battery (2026).

[89] O. Castaños, R. López-Peña, J. G. Hirsch, and E. López-Moreno, Classical and quantum phase transitions in the lipkin-meshkov-glick model, *Phys. Rev. B* **74**, 104118 (2006).

[90] S. Campbell, G. De Chiara, M. Paternostro, G. M. Palma, and R. Fazio, Shortcut to adiabaticity in the lipkin-meshkov-glick model, *Phys. Rev. Lett.* **114**, 177206 (2015).